


# Structure-based analysis and evolution of a monomerized red-colored chromoprotein from the *Olindias formosa* jellyfish

Le Zhai<sup>1,2</sup> | Ryosuke Nakashima<sup>2</sup> | Hajime Shinoda<sup>2</sup> | Yoshimasa Ike<sup>2,3</sup> | Tomoki Matsuda<sup>2,3</sup> | Takeharu Nagai<sup>1,2,3</sup> 

<sup>1</sup>Graduate School of Frontier Bioscience, Osaka University, Suita, Japan

<sup>2</sup>SANKEN (The Institute of Scientific and Industrial Research), Osaka University, Ibaraki, Japan

<sup>3</sup>Department of Biotechnology, Graduate School of Engineering, Osaka University, Suita, Japan

## Correspondence

Takeharu Nagai, Department of Biomolecular Science and Engineering, SANKEN (The Institute of Scientific and Industrial Research), Osaka University, F-301 Mihogaoka 8-1, Ibaraki, Osaka 567-0047 Japan.  
Email: ng1@sanken.osaka-u.ac.jp

## Funding information

Japan Science and Technology Corporation, Grant/Award Numbers: JPMJCR15N3, JPMJCR20E4; Ministry of Education, Culture, Sports, Science and Technology, Grant/Award Number: 18H05410

**Review Editor:** Aitziber L. Cortajarena

## Abstract

GFP-like chromoproteins (CPs) with non-fluorescence ability have been used as bioimaging probes. Existing CPs have voids in the optical absorption window which limits their extensibility. The development of new CP color is therefore ongoing. Here, we cloned CPs from the jellyfish, *Olindias formosa*, and developed a completely non-fluorescent monomeric red CP, R-Velour, with an absorption peak at 528 nm. To analyze the photophysical properties from a structural aspect, we determined the crystal structure of R-Velour at a 2.1 Å resolution. R-Velour has a *trans*-chromophore similar to the green fluorescence protein, Gamillus, derived from the same jellyfish. However, in contrast to the two coplanar chromophoric rings in Gamillus, R-Velour has a large torsion inducing non-fluorescence property. Through site-directed mutagenesis, we surveyed residues surrounding the chromophore and found a key residue, Ser155, which contributes to the generation of four-color variants with the bathochromic and hypsochromic shift of the absorption peak, ranging from 506 to 554 nm. The recently proposed spectrum shift theory, based on the Marcus–Hush model, supports the spectrum shift of these mutants. These findings may support further development of R-Velour variants with useful absorption characteristics for bioimaging, including fluorescence lifetime imaging and photoacoustic imaging.

## KEYWORDS

absorption shift, chromophore, chromoprotein, flower hat jellyfish, fluorescent protein

**Abbreviations:** CP, chromoprotein; GFP, green fluorescent protein; FP, fluorescent protein; FLIM, fluorescence lifetime imaging microscopy; FRET, Förster resonance energy transfer; PAI, photoacoustic imaging; *E. coli*, *Escherichia coli*; StEP, staggered extension process; R-Velour, Red GFP-like chromoprotein with very low quantum yield and visible color.

## 1 | INTRODUCTION

The green fluorescent protein (GFP) present in *Aequorea victoria*, avGFP, was first scientifically demonstrated as a

This is an open access article under the terms of the Creative Commons Attribution-NonCommercial-NoDerivs License, which permits use and distribution in any medium, provided the original work is properly cited, the use is non-commercial and no modifications or adaptations are made.

© 2022 The Authors. *Protein Science* published by Wiley Periodicals LLC on behalf of The Protein Society.

genetically encodable fluorescent tag. Since then, protein engineering of fluorescent proteins (FPs) has increased markedly to optimize their photophysical properties, resulting in diverse FP variants with notable features.<sup>1</sup> For FP engineering, structural information obtained by crystal structure analysis has contributed to color-tuning,<sup>2</sup> monomerization,<sup>3</sup> enhancement of quantum yield,<sup>4</sup> and the study of photoswitching mechanisms.<sup>5</sup> Non-fluorescent chromoproteins (CPs) homologous to FPs have also attracted attention. The structure of some CPs is composed of 11-stranded  $\beta$ -barrel and two internal  $\alpha$ -helices that embed the non-coplanar *trans*-chromophore with the same topology as the FPs with  $\beta$ -barrel fold so-called  $\beta$ -can.<sup>6</sup> Owing to their high light absorption efficiency and non-fluorescence properties, CPs have been preferentially applied as an acceptor of genetically encoded indicators for fluorescence lifetime imaging microscopy (FLIM)-based on Förster resonance energy transfer (FRET),<sup>7</sup> which requires only donor fluorescence for FRET detection.<sup>8</sup> Additionally, CPs have been applied to probes for photoacoustic imaging (PAI), enhancing visualization depth in biological tissues compared to fluorescent imaging. In PAI, light-excited molecules release energy through nonradiative relaxation, increasing local temperature and pressure and resulting in the propagation of photoacoustic waves. CPs also show higher efficiency of photoacoustic signal generation due to the absence of radiative relaxation and significantly increased photostability.<sup>9</sup>

Currently reported CPs derived from naturally existing *Anthozoa* exhibit yellow-green to orange light absorption (560–610 nm).<sup>10–15</sup> These CPs exist as tetramer, and when fused with the protein of interest, they may disturb the subcellular localization and function of target proteins. To avoid such problems, monomeric blue CP Ultramarine was developed by introducing mutations into the oligomeric interface of CP Rtm5 ( $\lambda_{\max} = 592$  nm).<sup>16</sup> CPs have also been developed by reducing the quantum yield of FPs. For example, REACH ( $\lambda_{\max} = 517$  nm),<sup>7</sup> dimVenus ( $\lambda_{\max} = 508$  nm),<sup>17</sup> and darkmCherry ( $\lambda_{\max} = 590$  nm)<sup>18</sup> were developed from popular FPs for bioimaging: EYFP, Venus, and mCherry, respectively. Recently, CPs with improved applicability to FLIM-FRET measurements have been developed by improvement from REACH and Ultramarine. REACH was improved with regards to the expansion of the absorption spectral range and further elimination of the residual fluorescence leading bleed-through into the fluorescence of the FRET donor. The color variants, ShadowG ( $\lambda_{\max} = 486$  nm)<sup>19</sup> and ShadowY ( $\lambda_{\max} = 519$  nm),<sup>20</sup> have been developed as acceptors of GFPs with much lower quantum yields (0.005 and 0.01, respectively) than parental REACH. ShadowR ( $\lambda_{\max} = 585$  nm)<sup>21</sup> was developed

from Ultramarine as the FRET acceptor for RFPs. Although directed evolution successfully yielded CPs with further decreased quantum yields in different colors, a well-characterized CP with an absorption wavelength from 520 to 560 nm in the current color window of the existing CP library, which can be potentially used as the FRET acceptor of YFP or OFP, is still lacking.<sup>22</sup> The development of completely non-fluorescent CPs from new organisms can potentially provide new color variants. This provides useful information on the development process, which would assist in establishing the general rule linking mutagenesis and absorption shift, providing a helpful guideline for CP diversification.

In this study, we investigated the CP expressed in the tentacles of the flower hat jellyfish, *Olindias formosa*. We recently isolated FP from the green fluorescent section of the tentacles and developed a novel GFP, Gamillus.<sup>23</sup> Non-fluorescent red-violet sections are also present at the distal portions of the green fluorescent sections in the tentacles. Thus, we expected the existence of a new red-violet CP with the potential to expand the CP absorption spectrum window. Here, we cloned a non-fluorescent CP with an absorption peak maximum at 528 nm from the tentacle. We developed a monomeric version of R-Velour and determined its 3D structure by X-ray crystallography and elucidated the photophysical differences with Gamillus, based on the crystal structures. To expand the CP color palette, we developed new color variants of O-Velour and M-Velour-554 with orange and magenta colors through site-directed mutagenesis and identified a key residue, Ser155, that confers the absorption-shift. A single replacement of Ser155 with hydrophobic residues can optimize the absorption spectrum of R-Velour in the range of 528–553 nm. These new color variants can compensate for the gaps in the current CP color window.

## 2 | RESULTS

### 2.1 | Molecular cloning of ofCP obtained from flower hat jellyfish

We cloned an unidentified CP gene from the tentacle sections of the flower hat jellyfish, *O. formosa*, with red-violet color and no fluorescence. A synthetic cDNA library was constructed using the mRNA extracted from the excised red-violet section of the jellyfish tentacle and cloned into the bacterial expression vector. Among the  $\sim 450,000$  colonies of *Escherichia coli* expressing the library, one red-violet colony and three faint red colonies were isolated. The CP with the highest extinction coefficient in the purified solution was selected as a novel red non-fluorescent CP and was designated as “ofCP” for

further study. The ofCP is composed of 229 amino acid residues and displays 49% and 42% amino acid sequence homology to dfGFP (origin of Gamillus) and anm2CP (origin of KillerRed), respectively (Figure S1).

## 2.2 | *In vitro* characterization of the photophysical property of ofCP

We evaluated the photophysical properties of the *E. coli* recombinant protein. The purified CP protein solution was red-violet in color, with no evident fluorescence under blue light irradiation. The optical absorption spectrum peak of ofCP at 528 nm was 24 nm longer than that of Gamillus. The molar extinction coefficient of ofCP at  $94,000 \text{ mM}^{-1} \text{ cm}^{-1}$  was slightly larger than that of Gamillus (Table 1). Interestingly, although both adopt the same chromophore tripeptide amino acid sequence, their optical properties differed. The undetectable quantum yield of ofCP implies its non-fluorescence emission property. The pH titration result indicated that ofCP was tolerant under weakly acidic physiological conditions ( $\text{p}K_a = 4.7$ ), similar to that of Gamillus ( $\text{p}K_a = 3.4$ ) (Table 1). The result of the size-exclusion chromatography indicated that ofCP tended to dimerize at high concentration in the overexpressed condition of the recombinant proteins in *E. coli* or mammalian cells (Figure 1d). Homodimerization hinders the normal function of the target protein and occasionally hampers its subcellular localization.<sup>24</sup> We then developed a monomeric CP form to address these potential complication.

## 2.3 | Monomerization of ofCP

We monomerized ofCP following a commonly applied strategy. We initially predicted a monomeric ofCP structure by homology modeling using the SWISS-MODEL server and superimposed the structure on each monomer in the published dimer structure of the fluorescent protein, KillerRed (PDB: 3gb3). A hydrophobic interface at the predicted interface promotes dimer formation. We

introduced the L154T mutation to reduce the hydrophobic interaction, as with the monomerization of Gamillus (Figure 1a,b). Although the mutant ofCP1.1 exhibited monomeric properties after size-exclusion chromatography, a relative decrease in the molar extinction coefficient ( $71,000 \text{ M}^{-1} \text{ cm}^{-1}$ ) occurred. To restore the molar extinction coefficient, we created a DNA library by random mutagenesis and screened for bacterial colonies with the desired dark red-violet color. Subsequently, a secondary DNA library was generated from the screened variants by DNA shuffling using the staggered extension process (StEP). The monomeric ofCP2 with restored molar extinction coefficient ( $91,000 \text{ M}^{-1} \text{ cm}^{-1}$ ) was successfully obtained (Figure 1c,d). We designated it as R-Velour abbreviated from “Red GFP-like chromoprotein with very low quantum yield and visible color”. The unmeasurable level of quantum yield and peak absorption wavelength of CP were preserved in R-Velour. The weaker acid resistance of light absorption ( $\text{p}K_a = 4.8$ ) than that of Gamillus was also preserved (Table 1).

## 2.4 | Crystal structure of R-Velour

The complete R-Velour gene is composed of 690 base pairs and encodes 229 amino acid residues. R-Velour shares 51% amino acid sequence homology with Gamillus, suggesting chromophore formation with the 60th to 62nd residues (Figure 2). Purified R-Velour protein with an N-terminal 6xHis-tag was crystallized and the 3D structure was determined using X-ray crystallography. The crystal belonged to  $I4_122$  space group, and the structure was refined to a final  $R_{\text{factor}}/R_{\text{free}}$  of 19.43/21.99%, at a resolution of 2.1 Å (PDB: 7cao; Table S1). R-Velour has the typical  $\beta$ -can fold of FP and is composed of an 11-stranded  $\beta$ -barrel, with each  $\beta$  sheet linked by a loop region and the circularized chromophore consisting of a tripeptide (Gln60-Tyr61-Gly62) located in the middle part of the  $\alpha 2$ -helix motif penetrating the central axis of the  $\beta$ -barrel (Figure 3a). Apparently, the two-ring chromophore of the R-Velour 4-(p-hydroxybenzylidene)-5-imidazolinone group consisted of a

**TABLE 1** Photophysical properties of ofCP, R-Velour, M-Velour-F, and Gamillus

Protein	$\lambda_{\text{max,abs}}^{\text{a}}$ (nm)	$\lambda_{\text{ex}}/\lambda_{\text{em}}^{\text{b}}$ (nm)	$\epsilon^{\text{c}}$ ( $\text{M}^{-1} \text{ cm}^{-1}$ )	$\Phi^{\text{d}}$	$\text{p}K_a^{\text{e}}$
ofCP	528	–	94,000	<0.001	4.7
R-Velour	528	–	91,000	<0.001	4.8
Gamillus	504	504/519	83,000	0.90	3.4

<sup>a</sup>Maximum absorbance wavelength.

<sup>b</sup>Excitation and emission peak wavelength.

<sup>c</sup>Molar extinction coefficient determined by alkali-denaturation method.

<sup>d</sup>Absolute fluorescence quantum yield determined by integrating sphere.

<sup>e</sup>pH at which absorption value becomes its half-maximal value.

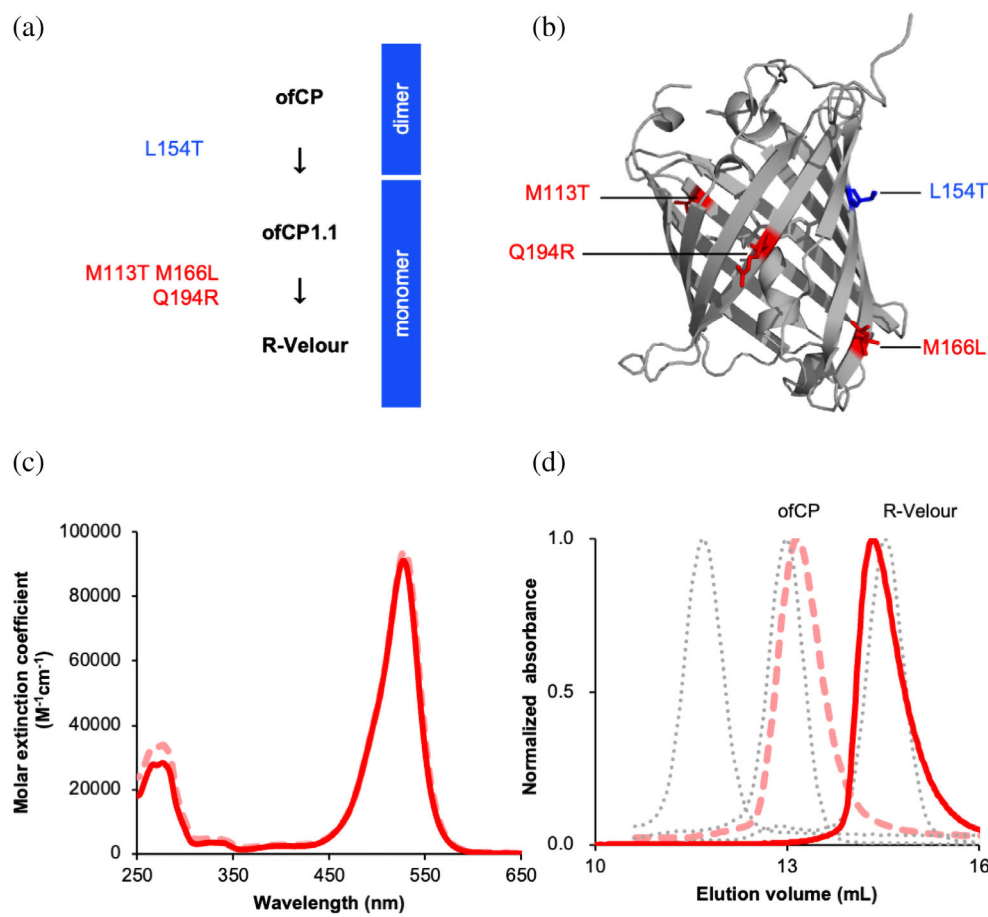


**FIGURE 1** Engineering of R-Velour from ofCP, and *in vitro* characterization of ofCP and R-Velour. (a) R-Velour lineage. (b) Positions of mutant amino acids during the directed evolution process were depicted on the X-ray crystal structure of R-Velour. The mutation for monomerization is represented in blue, and those for improved light absorption in red. (c) Molar extinction coefficient spectra of ofCP (rose dash line) and R-Velour (red solid line), measured at 30  $\mu\text{M}$ , pH 7.5 at 25°C.

(d) Size-exclusion chromatography for protein oligomerization analysis of ofCP (rose dash line) and R-Velour (red solid line). The dash gray lines from left to right represent the standard curves of the tetramer (DsRed), the dimer (KillerRed), and the monomer (mCherry), respectively

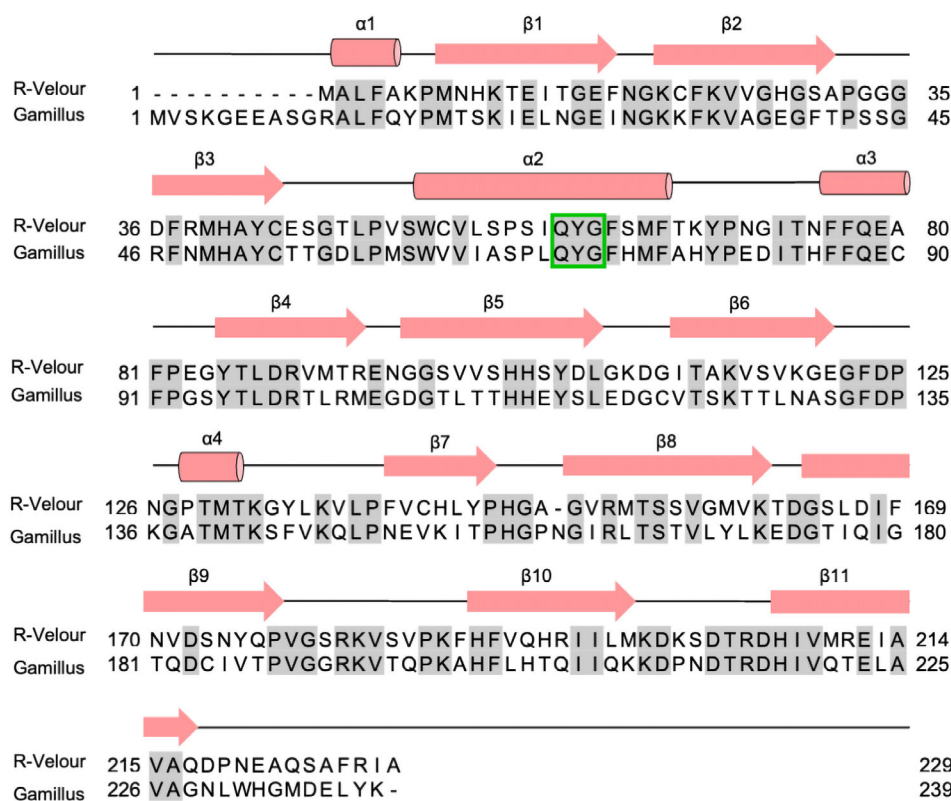


**FIGURE 2** Alignment of the amino acid sequences of GFP-like proteins of R-Velour and Gamillus from *Olindias formosa*. Identical residues between R-Velour with Gamillus are boxed in gray. The residues in the tri-peptide chromophore are indicated by the green frame. The secondary structure elements based on R-Velour are included above the alignment



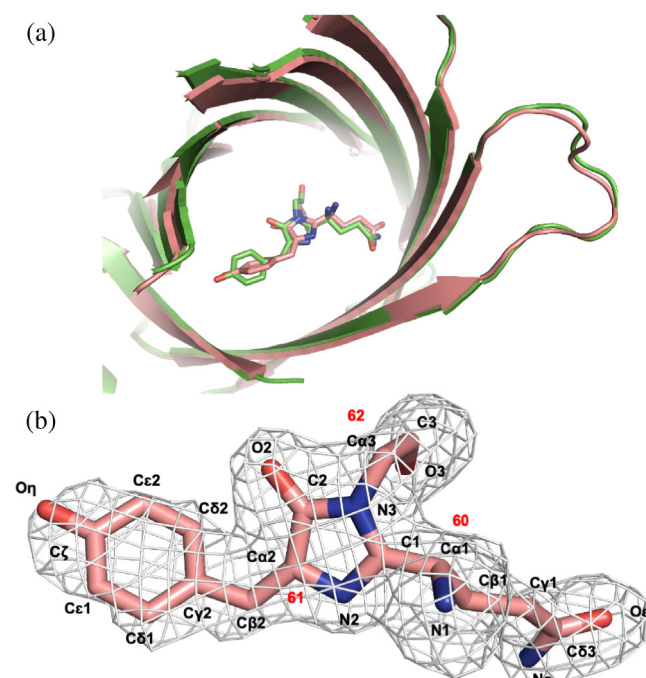


**FIGURE 3** Molecular structures of R-Velour determined by X-Ray crystallography. (a) Superimposed structure of R-Velour (salmon; PDB: 7cao) and Gamillus (green; PDB: 5y00). (b) The electron density map ( $2Fo-Fc$ ), contoured at  $1.0\sigma$ , is depicted as a gray mesh; the R-Velour chromophore is represented as a stick model (Salmon, carbon; Red, oxygen; Blue, nitrogen). Bold red numbers indicate the locations of  $C\alpha$  atoms in the amino acids Gln60, Tyr61, and Gly62 of R-Velour

central imidazolinone moiety with a *p*-hydroxybenzylidene substituent and adopts a *trans*-conformation between the  $C\alpha_2$ - $C\beta_2$  bond, as with Gamillus (Figure 3b). Similar to other GFP-like proteins,<sup>25</sup> the five-membered ring heterocyclic imidazolinone is presumed to be generated by a nucleophilic attack at the carbonyl group of Gln60, from the amide nitrogen of Gly62. Subsequently, the  $\pi$ -electron conjugated system is extended by further oxidation of the  $C\alpha_2$ - $C\beta_2$  bond in the Tyr61 moiety.

## 2.5 | Chromophore environment of R-Velour

We investigated the chromophore environment of R-Velour, which involved hydrogen bond network and van der Waals contacts (Figures 4, S2–S4, Table S2). The phenolate oxygen of the chromophore directly formed hydrogen bonds with a water molecule and Ser155 in the  $\beta_8$ -strand. Hydrogen bonds similar to that of the chromophore phenolate oxygen exist in Gamillus as bonds with a water molecule and Ser166 (Figure 4a,b). These

hydrogen bonds suggest stabilization of the *trans* chromophore. Meanwhile, extended hydrogen bond networks via the water molecule toward Met153 in the  $\beta_8$ -strand, and Ser173 in the  $\beta_9$ -strand, further stabilized the chromophore phenolic ring (Figure 4a). Because the water molecule is separated from bulk water and protects the protonation of chromophore phenolate oxygen by hydrogen bond formation in Gamillus (Figure 4b), it is considered to tolerate low pH ( $pK_a = 3.4$ ). A similar, but weakened effect was also present in R-Velour ( $pK_a = 4.8$ ). Moreover, both R-Velour and Gamillus have an identical arrangement of the highly conserved Arg89 and 99, and Glu212 and 223 residues, which form hydrogen bonds with O2 and N2 in the imidazolinone moiety (Figure 4c,d).

R-Velour chromophore has the small number of hydrogen bonds relative to that of Gamillus in glutamine- and glycyl moiety. The major difference is the lack of hydrogen bonds from the  $N\epsilon$  atom of the Gln60 moiety in R-Velour, where hydrogen bonds network among the corresponding atom of the Gln70 moiety, Phe47 and water molecules are formed in Gamillus. Furthermore, the O3 atom of the Gly62 moiety in R-Velour, whose corresponding atom of the Gly72 moiety in Gamillus forms hydrogen bonds with Pro68, His113, Tyr115, Ser124, and a water molecule, links with only one residue, Glu212, through a water molecule (Figure 4e,f). Conversely, most of the residues clustered around the chromophore in R-Velour only formed van der Waals contacts with the chromophore without forming hydrogen bonds, in contrast to a small number of van der Waals contact residues in Gamillus (Figure S4 and Table S2).

Supported by these interactions with surrounding residues, the chromophore in R-Velour exhibited an apparent non-coplanar conformation with noticeable dihedral angle distortion, which is a typical CP feature. Torsion angles, “tilt” ( $\tau$ ) and “twist” ( $\varphi$ ), calculated to evaluate the relative orientation of the two rings in the chromophore indicates that the trend of the off-coplanar chromophore of R-Velour is mainly due to the large  $\varphi$  ( $41.4^\circ$ ) angle, rather than the small  $\tau$  ( $-9.1^\circ$ ) angle (Figure 5a). The  $\varphi$  of R-Velour is much larger than that of Gamillus ( $9.5^\circ$ ), and the chromophore phenolic ring of the R-Velour is extruded from the plane of the imidazolinone moiety. This is due to steric hindrance from the bulky side chain of Phe140 in the  $\beta_7$ -strand, and Arg89 in the  $\beta_4$ -strand (Figure 5b). As for Gamillus, the corresponding residues, Asn150 and Arg99, do not disturb the coplanarity of the chromophore (Figure 5b). The mutagenesis results revealed that the Phe140 was considered a key factor influencing non-fluorescent properties. Replacement of Phe140 and its adjacent residue with other amino acids

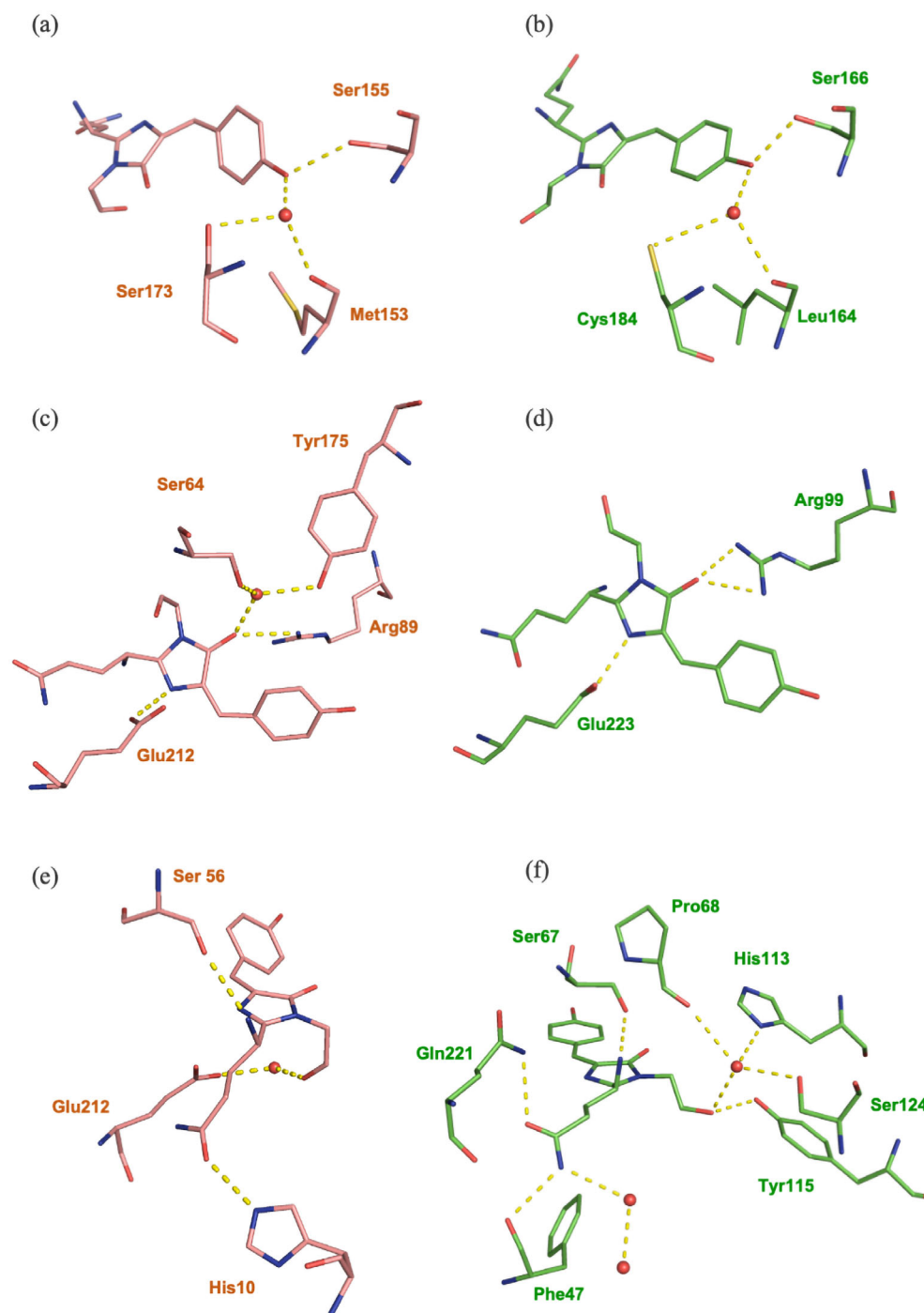


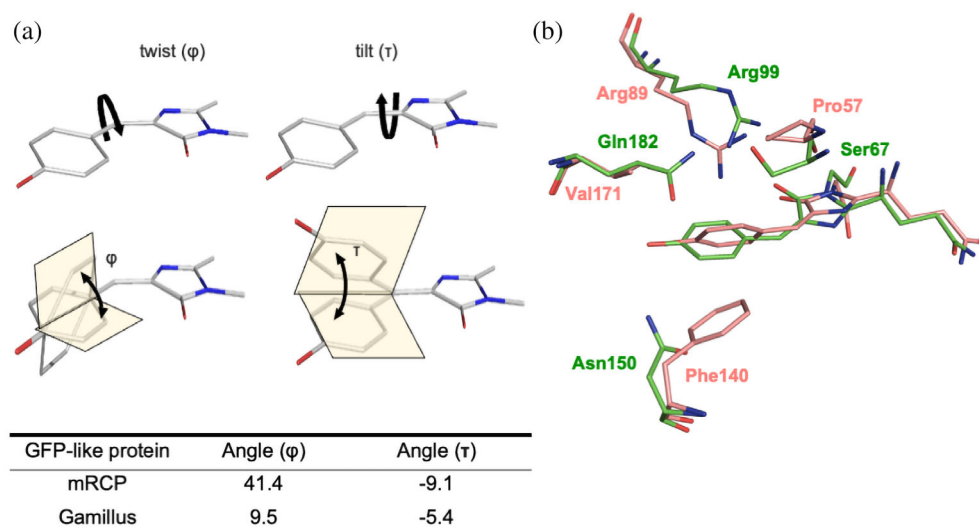
**FIGURE 4** Crystal structure of R-Velour (PDB: 7cao) (a, c, e) and Gamillus (PDB: 5y00) (b, d, f), in their nearest chromophore environment with hydrogen bond networks. The chromophore environment is depicted in a stick representation for R-Velour (salmon) and Gamillus (green). Hydrogen bond interactions are shown as yellow dashed lines and water molecules as red spheres. Insufficient hydrogen bond environment is indicated in the R-Velour chromophore

caused R-Velour to fluoresce (Supplementary Note 1). Additionally, the relatively long distance between Val171 in the  $\beta$ 9-strand and Pro57 in the  $\alpha$ 2-helix of R-Velour provides sufficient space to accommodate the distorted hydroxybenzylidene group. In Gamillus, Gln182 and Ser67 are in proximity through hydrogen bond interactions, which restricts chromophore torsion to maintain coplanarity (Figure 5b).

We also considered the chromophore flexibility by comparing the B-factors in the crystal structure

(Figure S5). Most of the atoms in the phenoxy moiety of the R-Velour's chromophore showed a higher B-factor than other atoms. B-factors of Glycyl- and Glutamine moieties follows that. The imidazolinone moiety with the smallest values exhibited a lower B-factor than the mean value of all atoms. For Gamillus, B-factors in all chromophore atoms were lower than the mean value of all atoms. These results suggest the higher motility of the phenoxy moiety of the R-Velour chromophore and the higher stability of the Gamillus chromophore. Taken

**FIGURE 5** Structure analysis of R-Velour, compared with Gamillus, based on their crystal structure. (a) Schematic illustration of “tilt” ( $\tau$ ) and “twist” ( $\varphi$ ) angles are shown in the upper part. Angle values of  $\tau$  and  $\varphi$  in R-Velour and Gamillus are shown in the table below. (b) Chromophore and closed residues of R-Velour (PDB: 7cao) and Gamillus (PDB: 5y00) are superimposed and colored in salmon and green, respectively



together, the non-fluorescence property of R-Velour with almost zero quantum yield might be attributed to the combination of the large torsion of the two chromophoric rings and higher motility of the phenoxy moiety.

## 2.6 | Site-directed saturation mutagenesis for color-alternation

According to the crystal structure of R-Velour, the internal residues of Met153 and Ser155 adjacent to the chromophore form a hydrogen bond network with the phenolic oxygen of the Tyr61 moiety to stabilize the *trans* chromophore (Figure 4a). Amino acid residues in the surrounding chromophore environment might affect its color properties,<sup>26</sup> thus we varied the 153rd to 155th residues in the  $\beta$ 8-strand to explore the new R-Velour color variants. As a result, two novel CP mutants, ofCP2.2 and ofCP2.4, with visible magenta and orange colors were

successfully obtained. The mutations introduced in ofCP2.2 and ofCP2.4 were T154V/S155T and M153A/T154L/S155G, respectively (Table 2). Because the residue, Thr154, with an outward side-chain is important to avoid dimerization of R-Velour, as previously mentioned, we introduced a 154T reverse mutation on ofCP2.2 and ofCP2.4. As a result, new color variants, M-Velour-554 and O-Velour, with mutations for only inward residues, were obtained (Figure 6a). As with R-Velour, the quantum yields of both color variants were undetectable. M-Velour-554, with a maximum absorption at 554 nm, has a 26 nm bathochromic shift from 528 nm for R-Velour. O-Velour, which mainly absorbed visible light at 506 nm, had a hypochromic shift of 22 nm, compared with R-Velour (Figure 6b and Table 2). The band at 392 nm in the absorption spectrum of O-Velour could be attributed to the neutral chromophore, which is identical to wild-type GFP and Gamillus.<sup>23,25</sup> Spectroscopic analysis indicated that M-Velour-554 and O-Velour have visible

**TABLE 2** Summary of R-Velour mutants

Protein	Abs <sup>a</sup> (nm)	Abs shift from R-velour (nm)	Residue's site			$\epsilon^b$ ( $M^{-1} cm^{-1}$ )	$\Phi^c$
			153	154	155		
R-Velour	528	–	M	T	S	91,000	<0.001
ofCP2.4	392, 506	–22	A	L	G	12,000, 15,000	<0.001
ofCP2.2	554	+26		V	T	61,000	<0.001
O-Velour	392, 506	–22	A		G	14,000, 20,000	<0.001
M-Velour-537	537	+9			A	72,000	<0.001
M-Velour-553	553	+25			V	72,000	<0.001
M-Velour-554	554	+26			T	86,000	<0.001

<sup>a</sup>Maximum absorbance.

<sup>b</sup>Molar extinction coefficient determined by alkali-denaturation method.

<sup>c</sup>Absolute fluorescence quantum yield determined by integrating sphere.

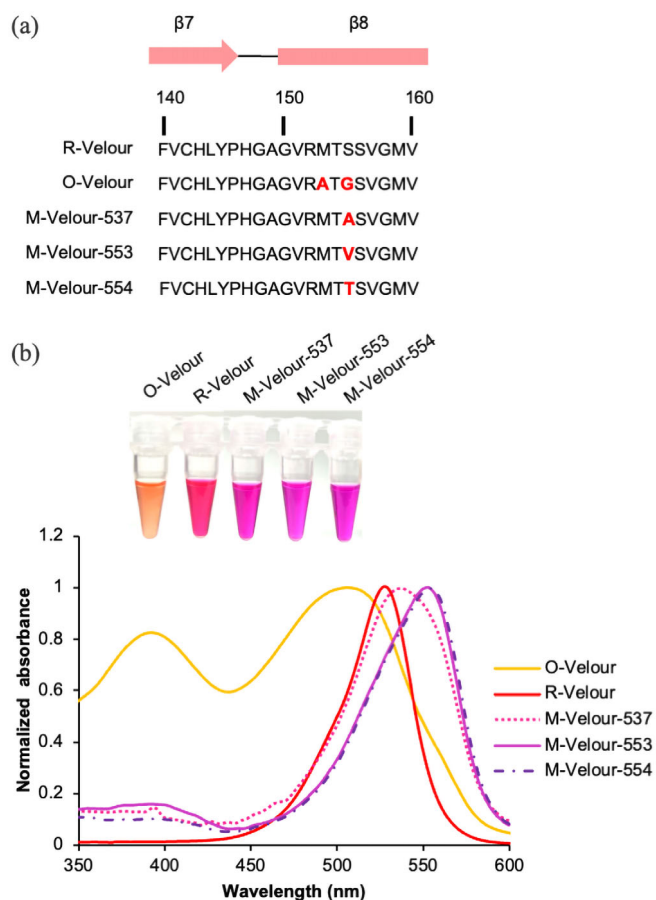


**FIGURE 6** Evolution of new color variants of O-Velour, M-Velour-537, M-Velour-553, and M-Velour-554 from R-Velour. (a) Amino acids sequence alignment (140th-160th). The mutations are highlighted in bold red. (b) Normalized absorption spectra of purified O-Velour, M-Velour-537, M-Velour-553, M-Velour-554, and R-Velour, which were measured at 10  $\mu\text{M}$ , pH 7.5 at 25°C

absorption with decreased molar extinction coefficients (86,000 and 20,000  $\text{mM}^{-1} \text{cm}^{-1}$ ) (Table 2). To further investigate the reasonable prediction of mutations causing absorption-shifts, we designed several amino acid substitutions at the 155th residue to observe any color changes. Magenta colored bathochromic-shifted mutants were obtained by introducing alanine and valine to replace Ser155. The CP mutant of S155V (M-Velour-553) exhibited a similarly large bathochromic shift (25 nm) absorption peak, while the S155A mutant (M-Velour-537) exhibited a smaller bathochromic shift (9 nm) (Figure 6b and Table 2).

### 3 | DISCUSSION

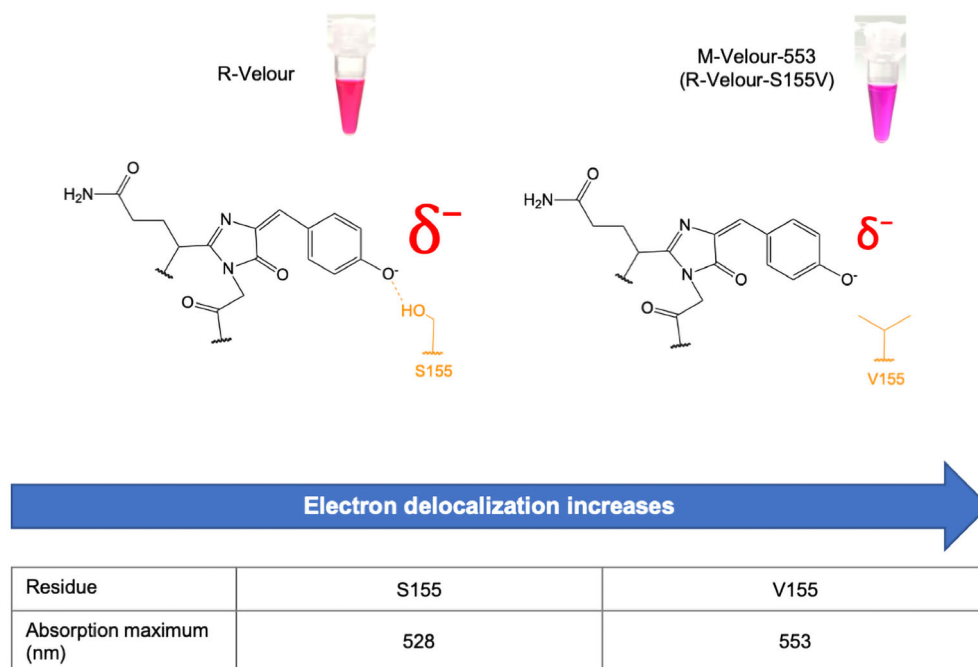
In the R-Velour mutation study, the substitution of Ser155 near the phenolic acid portion of the chromophore effectively affected the absorption peak shift. A

similar absorption peak shift was also reported for wild-type *A. victoria* GFP, and mutational studies have focused on the residues proximal to the chromophore, including Thr203.<sup>27</sup> Wild-type GFP exhibits near-ultraviolet and visible absorption peaks around 397 nm and 477 nm, corresponding to the neutral and anionic forms of the chromophore, respectively. According to mutational studies of the wild-type GFP, the anionic form is susceptible to mutations in the residues proximal to the chromophore, in contrast to the neutral form. Substitution of Thr203 with the aliphatic mutations of Val and Ile, which possibly disturbed hydrogen bonds with the chromophore, caused a bathochromic shift in the absorption peak of the anionic chromophore, ranging from 477 to 502 nm. Boxer et al. theoretically explained the trend in the absorption shift among GFP mutants, based on the resonance color theory derived from the Marcus–Hush model.<sup>28,29</sup> The authors treated the anionic GFP chromophore as a mixed-valence compound with superposition of two resonance forms, the phenolate- and the imidazolinone ring, both of which have charged localization centers on the oxygen atom (Figure S6a). The authors concluded that the absorption peak shift of the anionic chromophore was related to the driving force, which is defined by the energy difference between the two resonance forms induced by the difference in electron affinity between the two chromophoric rings. They claimed that charge destabilization on the phenolate, caused by changes such as the decline of hydrogen bonds,  $\pi - \pi$  stacking, and attachment of electron-donating groups, leads to a bathochromic shift of the absorption peak by reduction of the driving force, which means the modulation of the affinity of rings for the negative charge becomes the same level (Figure S6b).

Based on the aforementioned mutational studies wild-type GFP, we considered that significant bathochromic-shift absorption of R-Velour mutants by single-site mutants of S155V (M-Velour-553) and S155T (M-Velour-554) may occur due to the destruction of the chromophoric hydrogen bond between Ser155 and phenolic oxygen, which decreased the localization of electron charge on the phenolic oxygen (Figure 7). The S155A mutant (M-Velour-537) contained a smaller hydrophobic side-chain mutation that may have difficulty forming hydrogen bonds, while the smaller bathochromic-shift suggests less delocalization of electron charge on phenolate oxygen. O-Velour, which contains double mutations of M153A/S155G, showed a 22 nm hypsochromic shift. The difference between O-Velour and two M-Velour mutants (M-Velour-553 and M-Velour-554) is due to the alternative hydrogen bond with a water molecule that fills the larger space prepared by the substitution of the smaller glycine. Such hydrogen bonds might maintain or



**FIGURE 7** The putative chromophore environment of the M-Velour-553 color variant is depicted in a chemical structure. Disruption of the hydrogen bond leads to electron delocalization (Size of  $\delta^-$ ) on the phenolic oxygen of the chromophore, causing the bathochromic shifted absorption as observed



enhance the effect of electron charge localized on the chromophore phenolic oxygen, resulting in a small bathochromic- or hypsochromic shift. Further determination of the structures of color variants is required to support this assumption.

Taken together, we identified one novel, completely non-fluorescent red CP, namely R-Velour, from the flower hat jellyfish (*O. formosa*) and determined its crystal structure to a 2.1 Å resolution. The R-Velour chromophore also adopts a non-coplanar *trans*-chromophore. Structure-based mutagenesis of R-Velour revealed that the 153rd and 155th residues are important for altering the absorption peak wavelength, and the 140th and 142nd residues are vital to fluorescence properties. This information supports the development of novel CP color variants for multi-color imaging to satisfy the demand of biosensors with wider color variation to visualize multiple physiological events by multimodal imaging using conventional optical imaging, FLIM, and PAI.<sup>20</sup> R-Velour exhibits strong light absorption and is completely non-fluorescent, and can therefore be a potential acceptor paired with the donor of GFP such as Gamillus, or YFP such as Venus, in FLIM-FRET.<sup>7</sup>

## 4 | MATERIALS AND METHODS

### 4.1 | Protein expression and purification

Isolation of ofCP from *O. formosa* was described in Supplementary Note 2. The gene encoding the CPs was inserted into the pRSET<sub>B</sub> vector, which is a plasmid

vector for high protein expression with a cleavable polyhistidine tag. The plasmid was then transformed into *E. coli* JM109(DE3) and spread over the surface of LB agar medium with 100 µg/mL ampicillin. After overnight incubation at 37°C, single colonies were inoculated into 200 mL of LB liquid medium containing carbenicillin (100 µg/mL), and cultured with vigorous shaking in an incubator at 37°C for 69 h. The harvested bacterial cell lysate by French Press G-M (Glen Mills Inc.) following by purification using Ni-NTA agarose affinity columns (QIAGEN). The purified protein was eluted with 2 mL of 200 mM imidazole buffer. A PD-10 desalting column (Cytiva) was used for buffer exchange of purified protein to 20 mM HEPES at a pH of 7.4. Size-exclusion chromatography (SEC), using ÄKTA (GE Healthcare) equipped with a Superdex200 10/30 (GE Healthcare) column, was used for further purification. Filtration using a 0.2 µm pore filter was conducted in advance to remove the impurities before loading the proteins onto the column. The same procedure was followed to identify the oligomerization status. Photophysical analysis was described in Supplementary Note 3.

### 4.2 | pH sensitivity measurement and pK<sub>a</sub> determination

The following solutions were selected as pH buffers: a 30 mM trisodium citrate and 30 mM borate solution, ranging from 2 to 4; a 30 mM trisodium citrate and 30 mM sodium tetraborate solution, ranging from 5 to 8; a 30 mM CHES and 30 mM CAPS solution, ranging

from 9 to 11; and a 10 mM trisodium phosphate solution, ranging from 12 to 13. The absorption spectrum was recorded using a Bio UV-Vis spectrophotometer (V-630 BIO, Jasco). The measured absorption intensities were plotted against pH. The  $pK_a$  was determined by fitting the data to the following generalized Henderson-Hasselbalch equation using Origin8 software (OriginLab):

$$A = \frac{A_1}{1 + 10^{n_{H1}(pK_a - pH)}}$$

$A_1$  is the absorption intensity of the anionic chromophore at the maximum plateau.  $n_{H1}$  is the apparent Hill coefficient.

### 4.3 | Crystallization and structure determination

SDS-PAGE was performed to determine the degree of purification. To prepare the protein concentration gradient (10, 15, and 20 mg/mL) for the crystallization experiment, the purified protein was collected and concentrated using a centrifugation column (Millipore). The crystallization condition for the purified protein sample was initially selected using broad range screening according to a sitting-drop vapor diffusion method and optimized by a hanging-drop vapor diffusion method. Optimal R-Velour crystals were obtained in buffer containing 14% PEG 3350, 200 mM tri-sodium citrate pH = 5.4, 600 mM NaCl, and 20 mM HEPES at a temperature of 20°C. The crystals were immersed in 20% (vol/vol) glycerol as a harvesting buffer for cryoprotection and frozen in liquid nitrogen. Diffraction data were collected by applying the BL44XU beamline at Spring-8, with an EIGER 16 M detector at 100 K. The diffraction data were processed and scaled using the XDS program package. Initial phasing of the crystals was performed by molecular replacement using KillerRed (PDB ID: 3gb3) as the search model. The structures were refined and remodeled using the programs REFMAC (CCP4i) and *Coot*. Figures were prepared using PyMOL software (<https://www.pymol.org/>). The B-factors were standardized using the following equation:

$$B_{\text{norm}} = (B - \langle B \rangle) / \sigma$$

where  $B$  is the original B-factor value,  $\langle B \rangle$  is the average of the B-factor (raw value) considered in a given structure, and  $\sigma$  represents the standard deviation.<sup>30</sup>

### 4.4 | Random mutagenesis, StEP, site-directed and saturation mutagenesis, and screening of libraries

Random mutagenesis and StEP for improving the extinction coefficient of CP1.1 was described in Supplementary Note 4. Site-directed and saturation mutagenesis based inverse PCRs were performed to generate the monomeric CP and R-Velour variants. Degenerate primers with randomized codons used in saturation research were purchased from Hokkaido System Science. The primers need to be phosphorylation in advance following by inverse PCR for DNA library amplification. The primers are listed in Table S3. To avoid transformation of the template DNA into *E. coli* JM109(DE3), the restriction enzyme, *DpnI*, was used to digest the methylated template DNA. The synthesized linear DNA plasmid was purified by phenol-chloroform extraction and ethanol precipitation. For ligation, 2  $\mu$ L of single strand plasmid was mixed with 0.5  $\mu$ L of T4 ligase (Promega), 2  $\mu$ L of 2 $\times$  Rapid Ligation Buffer (Promega), and 1.5  $\mu$ L of H<sub>2</sub>O, at room temperature. After incubation for 15 min, 8  $\mu$ L of the ligation solution was transformed into *E. coli* JM109(DE3). Approximately 15,000 colonies were prepared and screened with the naked eye under ambient light in each round of mutagenesis to check the CP color variants.

### 4.5 | Phylogenetic analysis

Amino acid identification and similarity assessment of CP and R-Velour was performed using the BLAST server ([https://blast.ncbi.nlm.nih.gov/Blast.cgi?PROGRAM=blastp&PAGE\\_TYPE=BlastSearch&LINK\\_LOC=blasthome](https://blast.ncbi.nlm.nih.gov/Blast.cgi?PROGRAM=blastp&PAGE_TYPE=BlastSearch&LINK_LOC=blasthome)). The sequence was aligned with hydrozoan FP sequences using the Clustal Omega online server, and sequence alignment graphics were generated using JalView software. The GenBank accession numbers for the aligned FPs are: dfGFP (*BBC28143*), Gamillus (*BBC28144*) and anm2CP (*AAR85352*).

### ACKNOWLEDGMENTS

We thank Kazuya Okuizumi (Kamo Aquarium, Japan) for kindly providing us with the flower hat jellyfishes, *O. formosa*. This work was performed using a synchrotron beamline BL44XU at SPring-8 under the Cooperative Research Program of the Institute for Protein Research, Osaka University. Diffraction data were collected at the Osaka University beamline BL44XU at SPring-8 (Harima, Japan) under proposal numbers 2018B6830, 2019A6928. This work was supported by the MEXT "Grant-in-Aid for Scientific Research on

Innovative Areas” “Singularity biology” (18H05410) to T.N., JST CREST Program (JPMJCR15N3 to T.N. and JPMJCR20E4 to T.M.).

## AUTHOR CONTRIBUTIONS

**Le Zhai:** Data curation (equal); formal analysis (equal); investigation (equal); writing – original draft (equal). **Ryosuke Nakashima:** Data curation (equal); formal analysis (equal); resources (supporting); validation (supporting). **Hajime Shinoda:** Data curation (supporting). **Yoshimasa Ike:** Data curation (supporting); investigation (supporting); resources (supporting). **Tomoki Matsuda:** Data curation (supporting); formal analysis (supporting); investigation (supporting); writing – review and editing (equal). **Takeharu Nagai:** Conceptualization (equal); investigation (equal); project administration (equal); resources (equal); supervision (equal); validation (equal); writing – review and editing (equal).

## DATA AVAILABILITY STATEMENT

The nucleotide sequence data of ofCP and R-Velour was deposited on DNA Data Bank of Japan (DDBJ) with accession number of *LC663961* and *LC663962*, respectively. The crystallographic data for R-Velour is deposited on Protein Data Bank Japan (PDBj) with the deposition numbers 7cao.

## ORCID

Takeharu Nagai  <https://orcid.org/0000-0003-2650-9895>

## REFERENCES

- Rodriguez EA, Campbell RE, Lin JY, et al. The growing and glowing toolbox of fluorescent and photoactive proteins. *Trends Biochem Sci.* 2017;42:111–129.
- Hense A, Nienhaus K, Nienhaus GU. Exploring color tuning strategies in red fluorescent proteins. *Photochem Photobiol Sci.* 2015;14:200–212.
- Hoi H, Howe ES, Ding Y, et al. An engineered monomeric *Zoanthus* sp. yellow fluorescent protein. *Chem Biol.* 2013;20:1296–1304.
- Goedhart J, von Stetten D, Noirclerc-Savoye M, et al. Structure-guided evolution of cyan fluorescent proteins towards a quantum yield of 93%. *Nat Commun.* 2012;3:751.
- Brakemann T, Weber G, Andresen M, et al. Molecular basis of the light-driven switching of the photochromic fluorescent protein Padron. *J Biol Chem.* 2010;285:14603–14609.
- Prescott M, Ling M, Beddoe T, et al. The 2.2 Å crystal structure of a pocilloporin pigment reveals a nonplanar chromophore conformation. *Structure.* 2003;11:275–284.
- Ganesan S, Ameer-Beg SM, Ng TT, Vojnovic B, Wouters FS. A dark yellow fluorescent protein (YFP)-based resonance energy-accepting Chromoprotein (REACH) for Förster resonance energy transfer with GFP. *Proc Natl Acad Sci U S A.* 2006;103:4089–4094.
- Yasuda R, Harvey CD, Zhong H, Sobczyk A, van Aelst L, Svoboda K. Supersensitive Ras activation in dendrites and spines revealed by two-photon fluorescence lifetime imaging. *Nat Neurosci.* 2006;9:283–291.
- Brunker J, Yao J, Laufer J, Bohndiek SE. Photoacoustic imaging using genetically encoded reporters: A review. *J Biomed Opt.* 2017;22:070901.
- Lukyanov KA, Fradkov AF, Gurskaya NG, et al. Natural animal coloration can be determined by a nonfluorescent green fluorescent protein homolog. *J Biol Chem.* 2000;275:25879–25882.
- Dove SG, Takabayashi M, Hoegh-Guldberg O. Isolation and partial characterization of the pink and blue pigments of pocilloporid and acroporid corals. *Biol Bull.* 1995;189:288–297.
- Gurskaya NG, Fradkov AF, Terskikh A, et al. GFP-like chromoproteins as a source of far-red fluorescent proteins. *FEBS Lett.* 2001;507:16–20.
- Shkrob MA, Yanushevich YG, Chudakov DM, et al. Far-red fluorescent proteins evolved from a blue chromoprotein from *actinia equina*. *Biochem J.* 2005;392:649–654.
- Chan MC, Karasawa S, Mizuno H, et al. Structural characterization of a blue chromoprotein and its yellow mutant from the sea anemone *Cnidopus japonicus*. *J Biol Chem.* 2006;281:37813–37819.
- Chiang CY, Lee CC, Lo SY, Wang AH, Tsai HJ. Chromophore deprotonation state alters the optical properties of blue chromoprotein. *PLoS One.* 2015;10:e0134108.
- Pettikiriarachchi A, Gong L, Perugini MA, Devenish RJ, Prescott M. Ultramarine, a chromoprotein acceptor for Förster resonance energy transfer. *PLoS One.* 2012;7:e41028.
- Matsuda T, Horikawa K, Saito K, Nagai T. Highlighted Ca<sup>2+</sup> imaging with a genetically encoded 'caged' indicator. *Sci Rep.* 2013;3:1398.
- Nakahata Y, Nabekura J, Murakoshi H. Dual observation of the ATP-evoked small GTPase activation and Ca<sup>2+</sup> transient in astrocytes using a dark red fluorescent protein. *Sci Rep.* 2016;6:39564.
- Murakoshi H, Shibata ACE, Nakahata Y, Nabekura J. A dark green fluorescent protein as an acceptor for measurement of Förster resonance energy transfer. *Sci Rep.* 2015;5:15334.
- Murakoshi H, Shibata ACE. ShadowY: A dark yellow fluorescent protein for FLIM-based FRET measurement. *Sci Rep.* 2017;7:6791.
- Murakoshi H, Horiuchi H, Kosugi T, et al. ShadowR: A novel chromoprotein with reduced non-specific binding and improved expression in living cells. *Sci Rep.* 2019;9:12072.
- Liljeruhm J, Funk SK, Tietscher S, et al. Engineering a palette of eukaryotic chromoproteins for bacterial synthetic biology. *J Biol Eng.* 2018;12:8.
- Shinoda H, Ma Y, Nakashima R, Sakurai K, Matsuda T, Nagai T. Acid-tolerant monomeric GFP from *Olindias formosa*. *Cell Chem Biol.* 2018;25:330–338.e7.
- Takemoto K, Matsuda T, Sakai N, et al. SuperNova, a monomeric photosensitizing fluorescent protein for chromophore-assisted light inactivation. *Sci Rep.* 2013;3:2629.
- Cubitt AB, Heim R, Adams SR, Boyd AE, Gross LA, Tsien RY. Understanding, improving and using green fluorescent proteins. *Trends Biochem Sci.* 1995;20:448–455.
- Chiang CY, Chen YL, Tsai HJ. Different visible colors and green fluorescence were obtained from the mutated purple chromoprotein isolated from sea anemone. *Mar Biotechnol (NY).* 2014;16(4):436–446.

27. Kummer AD, Wiehler J, Rehabe H, Kompa C, Steipe B, Michel-Beyerle ME. Effects of threonine 203 replacements on excited-state dynamics and fluorescence properties of the green fluorescent protein (GFP). *J Phys Chem B*. 2000;104(19), 4791–4798.
28. Lin CY, Romei MG, Oltrogge LM, Mathews II, Boxer SG. Unified model for photophysical and electro-optical properties of green fluorescent proteins. *J Am Chem Soc*. 2019;141:15250–15265.
29. Romei MG, Lin CY, Mathews II, Boxer SG. Electrostatic control of photoisomerization pathways in proteins. *Science*. 2020; 367:76–79.
30. Sun Z, Liu Q, Qu G, Feng Y, Reetz MT. Utility of B-factors in protein science: Interpreting rigidity, flexibility, and internal motion and engineering thermostability. *Chem Rev*. 2019;119:1626–1665.

## SUPPORTING INFORMATION

Additional supporting information may be found in the online version of the article at the publisher's website.

**How to cite this article:** Zhai L, Nakashima R, Shinoda H, Ike Y, Matsuda T, Nagai T. Structure-based analysis and evolution of a monomerized red-colored chromoprotein from the *Olindias formosa* jellyfish. *Protein Science*. 2022; 31(5):e4285. <https://doi.org/10.1002/pro.4285>